Report IDM reference No.	EFDA_D_2NXTNT	Version: see IDM

Final Report

on Activity

{DTT1-ADC.P-1 "Fluid models"}

		Deliverable-ID[1]	DTT1-ADC.P-1-T001-D001
Work Package	*WPADC*	**Date**	*28.5.2020*
Project Leader	*Fulvio Militello*		
Activity Title	*Fluid models*		
Activity Ref. No.	*WPADC.P-1*	**TS IDM-link**	EFDA_D_2NXTNT
Project Manager	Leena Aho-Mantila, Marco Wischmeier		
RU(s)	CCFE, ENEA, EPFL, IPP, VTT		

Report Review & Approval	
IDM role	**Name(s)**
Author	*Leena Aho-Mantila*
Co-author(s)	*David Coster, Tilmann Lunt, Fabio Subba, Mirko Wensing, Marco Wischmeier, Lingyan Xiang*
Reviewer(s)	*Fulvio Militello*
PMU Reviewer	*Michael Reinhart*
Approver	*Fulvio Militello*

[X] Study / Assessment [ ] Procurement / Commissioning of Hardware [ ] Industry

[ ] Use of Facility [ ] Other *{please specify}*

Executive Summary

The 2019 P-1 work focused on the following 3 activities: (i) redefining and standardizing the assumptions and run parameters used for simulating the edge plasmas of the ADCs, (ii) updating the computational meshes and wall geometries to model the 2018 engineering designs, and (iii) performing parameter scans with varying fueling and impurity seeding levels to identify possible operational regimes in all configurations.

In line with the first activity (i), we decided to carry out all the 2019 simulations using the same code, namely the SOLPS-ITER code package. With SOLPS-ITER it is possible to model all single-null geometries, namely the SN, XD and SX configurations, as well as two geometries

[1] One *Deliverable Report* shall be submitted for each deliverable e.g. Study Report, Commissioning Report, Final Assessment Report, Technical Acceptance Report, Procurement Report, etc.

with more than one X-point: the DN and the SF- configurations. This means that in activity (ii) we were able to create computational meshes for all of the 2018 engineering designs apart from the SF+ configuration.
In activity (iii), we carried out an extensive set of simulations using a simplified, fluid description of the neutrals. The D gas puff levels were varied to cover at least $n_{e,sep} = 0.4…0.6n_{GW}$ (and in some cases a wider range of $n_{e,sep}$), and the Ar impurity seeding levels were varied resulting in radiative regimes ranging from pure D radiation to combined D+Ar radiation with as high radiated power fraction as possible.
Possible operational points satisfying the criteria $T_{e,target} < 5$ eV, $q_{target} < 10$ MW/m^2 and $n_{e,sep} < 0.6n_{GW}$ were identified in all configurations apart from the SF-, for which converged solutions with high Ar seeding rate are still pending. Indeed, all of the configurations require Ar seeding to reach acceptable conditions at all active targets within the specified upstream density limit. Asymmetric target solutions were obtained in all configurations, with the most critical target conditions obtained in some cases on the low-field-side (SN, SX, SF-), on the high-field-side (XD, SX), or symmetrically at both lower targets (DN, with significant up-down asymmetry). Future efforts should consider the effects of kinetic neutrals and drifts on the asymmetries, and focus on further characterizing and understanding the differences in the operational spaces between the configurations.

Table of contents

1 Description

1.1 Fluid modelling setup

One of the main goals of the 2019 fluid modelling task was a careful reassessment and standardization of the inputs used in the fluid simulations. Modelling efforts focused on using the SOLPS-ITER code package to simulate all available configurations, based on the most recent complete set of engineering designs obtained in 2018. As a first step, we decided to perform extensive parameter scans with varying fueling and impurity puffing levels to identify and compare the operational windows between the configurations. To optimize our resources, we decided to carry out these large matrix scans using a *fluid neutral model* in the simulations. Later on, it is planned to complement the results by performing simulations with a *kinetic neutral model* for selected operational points for verification and more detailed physics analyses, see Section 1.3.

Table 1 summarizes the input assumptions agreed to be used in the simulations with a fluid neutral model. These specifications were discussed and decided in a technical meeting held at IPP Garching in March 2019.

Table 1: Assumptions used for the set-up of SOLPS-ITER simulations of ADCs with fluid neutrals (2019)

Input parameter/ simulation specification	**2019 decision**
Code:	
SOLPS-ITER version	3.0.6 develop, B2.5 versions: SN, XD: 3.0.6-336-g7dd1b193 SX: 3.0.6-283-g59d7c19-dirty DN: 3.0.6-297-gf39e16a2 SF: 3.0.6-289-g87b0815f
Mesh (SN, XD, SX):	
Grid resolution	96x36
SOL width, outer midplane	8-9 cm
Core width, outer midplane	10 cm
PFR width, X-point	same as SOL width in this region
Species set-up:	
Neutral model	fluid
Fuel species	D
Intrinsic impurities	He
Puffed impurities	Ar (bundled into 3 charge state groups)
Sources/sinks:	
Core boundary particle sources	$3.5E22s^{-1}$ D-atoms, $7E20s^{-1}$ He-atoms
PFR boundary particle sinks	1% of neutrals absorbed (“pumped”)
Core boundary energy sources	150 MW equally shared by ions and electrons
Radial transport:	
end of core values, start of SOL values (outer midplane position)	- 5mm, 0 mm
D	0.1 m^2/s, 0.1 m^2/s
χ_e	0.1 m^2/s, 0.3 m^2/s
χ_i	0.1 m^2/s, 0.3 m^2/s
viscosity	0.2 m^2/s, 0.2 m^2/s
λ_q	~3 mm
Parallel transport:	
ion heat flux limiter	10^5

electron heat flux limiter	0.2
viscosity flux limiter	0.375

1.2 Results obtained from the fluid neutral matrix scans

1.2.1 SN

1.2.1.1 Mesh and other configuration-specific settings

The mesh generation for the SN cases is relatively standard using the SOLPS-ITER chain tool, and did not raise any significant problems. We selected a 96 (poloidal) × 36 (radial) mesh, optimized to have about 5 cells in the first radial energy decay length from the OMP separatrix assumed to be λ_E~3 mm). Figure 1 shows a magnification of the mesh obtained in the divertor region. In the poloidal direction, the mesh is refined near the targets, aiming at a resolution of ~ 1 mm close to the solid surfaces.

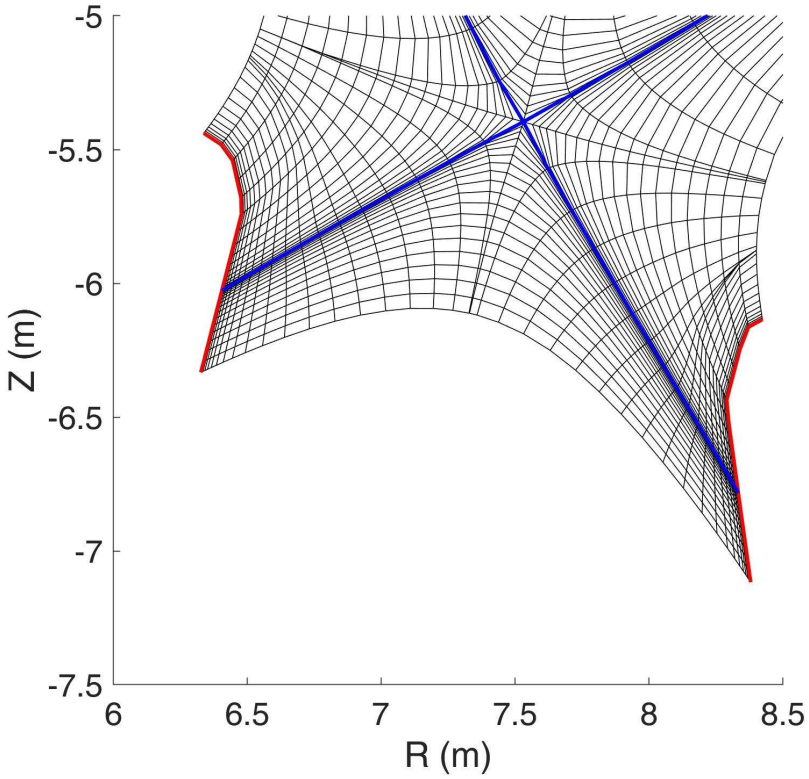

Figure 1: Magnification of the SN mesh close to the divertor region

1.2.1.2 Runs and operational space

Our parameter space was defined by the ranges of deuterium puff (within limits 4.66×10^{23} s^{-1} and 6.24×10^{24} s^{-1}), and impurity (Argon) puff (within limits 0.0 s^{-1} and 3.5×10^{21} s^{-1}). Figures 2 and 3 show the peak electron temperature along the inner and outer target plates. The actual simulations obtained are marked by the red circles, all the other points being obtained by a proper interpolation. As often happens in SN modeling and experiments, the outer target shows a temperature considerably larger than the inner one, and constitutes, in this respect, the actual bottleneck for divertor operation. In our current parameter scan we have found 1 converged

solution which satisfies the criteria $T_{e,target} < 5$ eV (solid contour line) and $n_{e,sep} < 0.6n_{GW}$ (dashed contour line).

When trying to run cases out of the colored region, the simulations crashed. At this stage, we have not done a systematic attempt at determine precisely the boundaries of the region where the simulations converge, so we did not accumulate points close to the plot boundaries. We did try, however, some simple tests to extend the convergence region, e.g. by reducing the time step by an order of magnitude, but this failed. Figure 4 shows the electron pressure at the OMP as a function of the Ar puff rate. We can clearly see that, at a sufficiently high level of impurity puff, the upstream pressure starts dropping quickly. The code stops converging at higher levels of Ar puff rate. This suggests that the boundary of the parameter space explored by the simulations does not depend on a numerical instability, but rather on an important change in the dominant physics processes. To give a reference value, the upstream pressure drop becomes noticeable (i.e. 10% of the total) when the total line radiation in the plasma is ~ 95 MW (63 %) of the total input power. The last converged point of the line corresponds to a total line radiation of ~ 100 MW (67 % of the total input power).

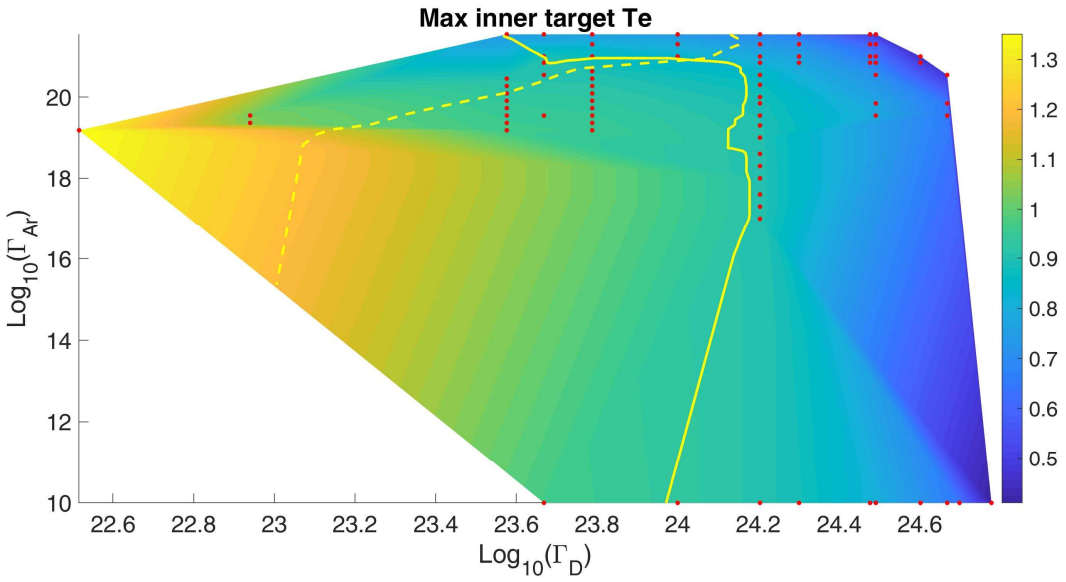

Figure 2: Inner target peak temperatures (eV) for the SN scan performed

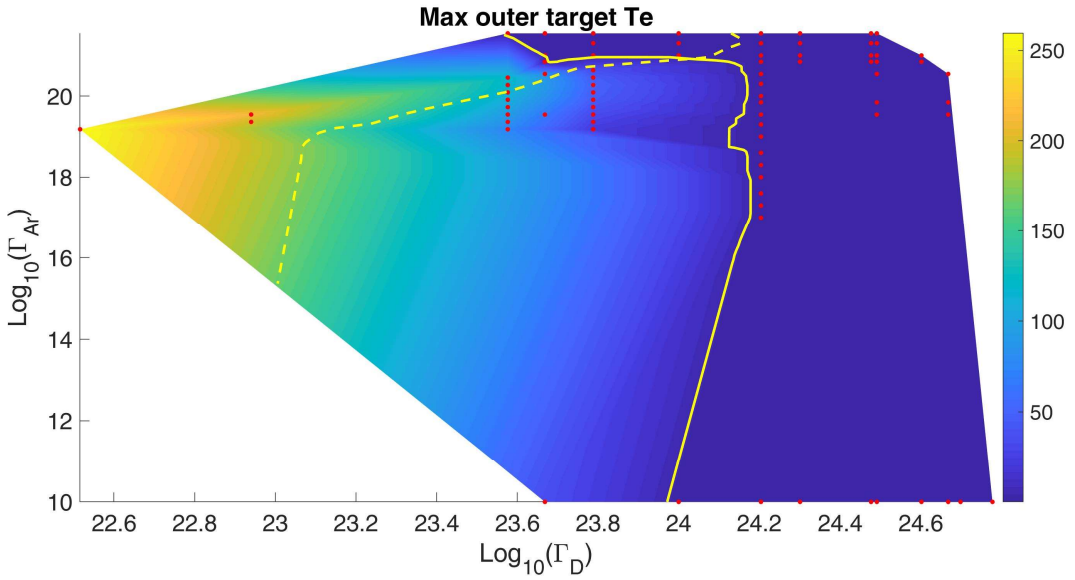

Figure 3: Outer target peak temperatures (eV) for the SN scan performed

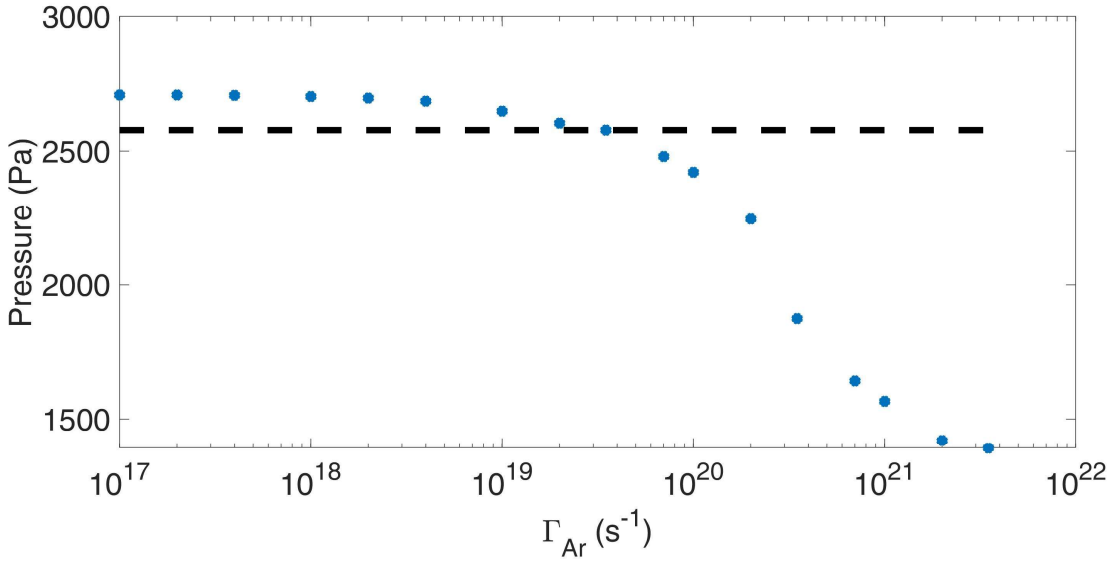

Figure 4: OMP electron pressure at a constant D puff rate of 1.60×10^{24} s^{-1}

1.2.2 XD

1.2.2.1 Mesh and other configuration-specific settings

From the topological point of view, the XD geometry is a special case of the SN, and the meshing procedure was quite similar to the one previously sketched. Figure 5 shows the mesh in the divertor region.

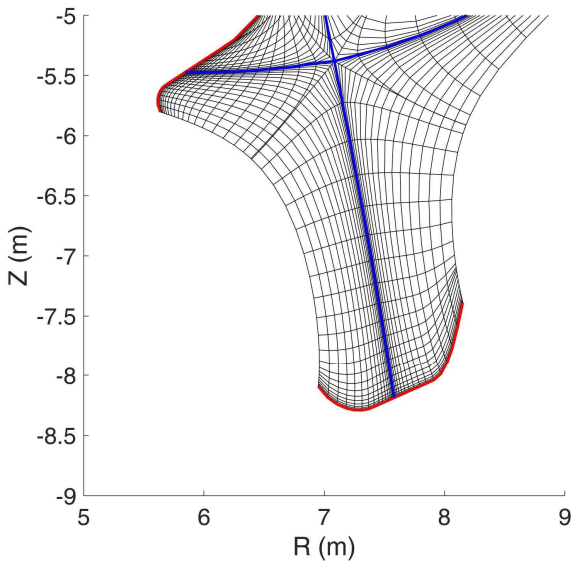

Figure 5: Mesh in the divertor region for the XD case

When running our scans, some cases did not fully converge, but relaxed over a stationary oscillating behavior, as exemplified in Figure 6. Although such oscillations may be substantial, as exemplified in the figure, they appeared in the boundary region of the operational space we explored, i.e. in region not interesting from a physics point of view (e.g. where the electron temperature is too large anyway to represent an interesting working point).

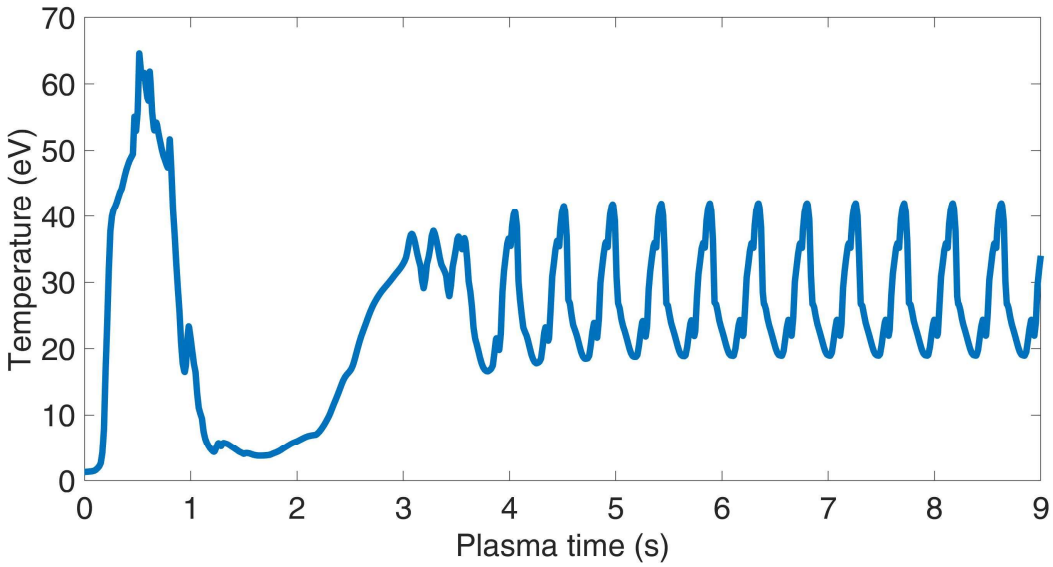

Figure 6: Example of oscillating behavior observed in some cases (here we show the inner target peak electron temperature)

1.2.2.2 Runs and operational space

The major differences between SN and XD configurations are (i) the longer connection length on the outer side and (ii) the flaring of the magnetic field lines close to the outer target, which helps to efficiently spread the deposited power. Both conditions point in the direction of favoring the outer target conditions with respect to the inner one. This is clearly reflected in Figures 7 and 8, which show the peak electron temperatures at the targets for the XD case. The major difference

with respect to the SN configuration is a complete reversing of the in/out asymmetry, with the inner target raising in some cases to temperatures larger than 200 eV (obviously not within a possible operating space), while the outer one stays always at a few eV at most. As shown in the figures, also for this case we selected a specific D puff level and explored it in detail. In this case, the maximum line radiation obtained was ~ 110 MW (73 % of the total).

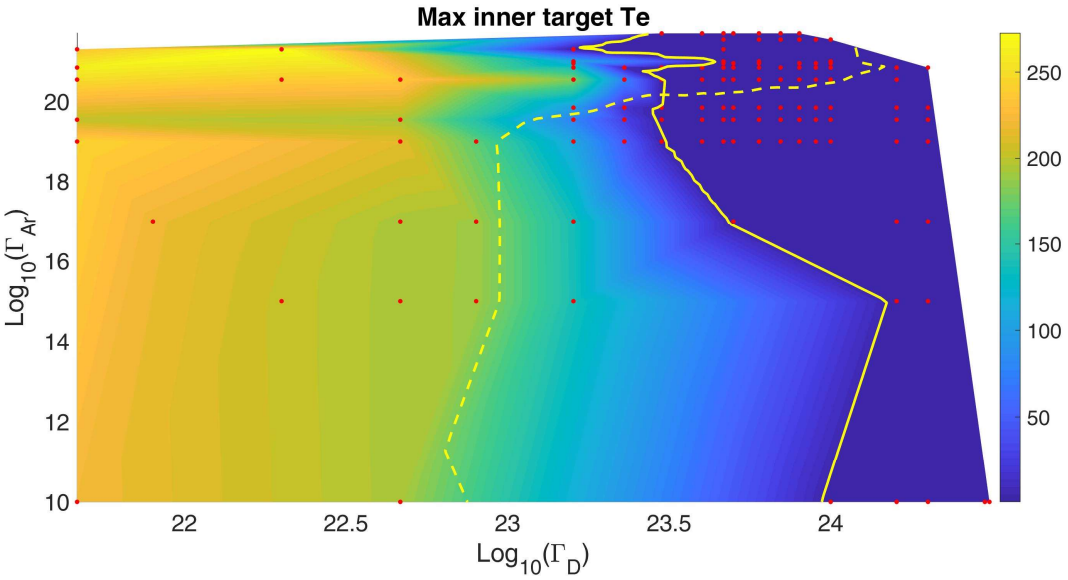

Figure 7: Inner target peak temperature for the XD case

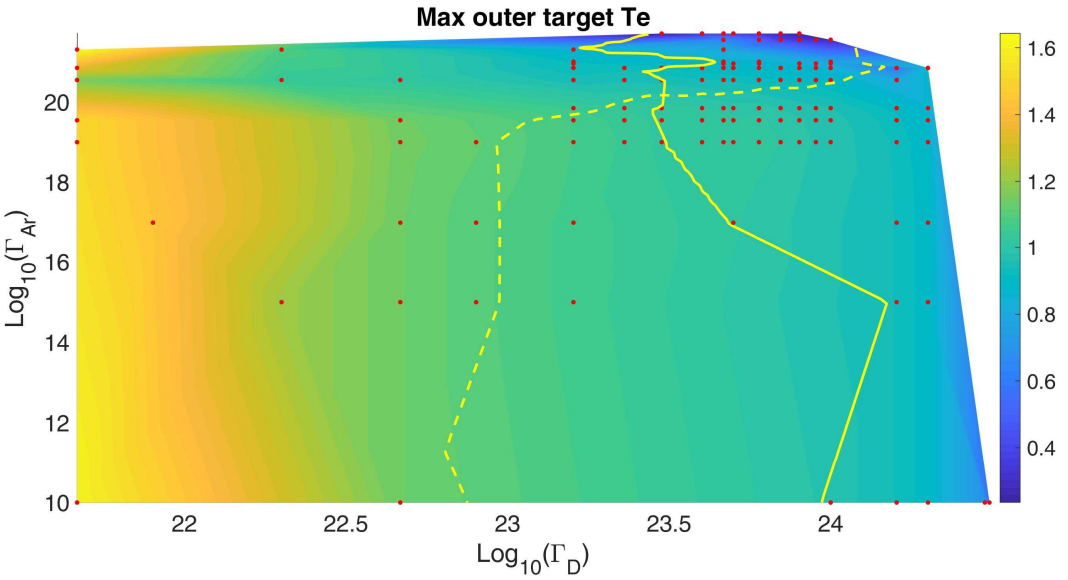

Figure 8: Outer target peak temperature for the XD case

1.2.3 SX

1.2.3.1 Mesh and other configuration-specific settings

There were 3 issues that needed to be tackled during setting up the simulations. The first was that the divertor targets needed minor modifications in order to produce orthogonal grid close to the target surface. The modification comparing to the original design for DEMO vacuum vessel is shown in Figure 9.

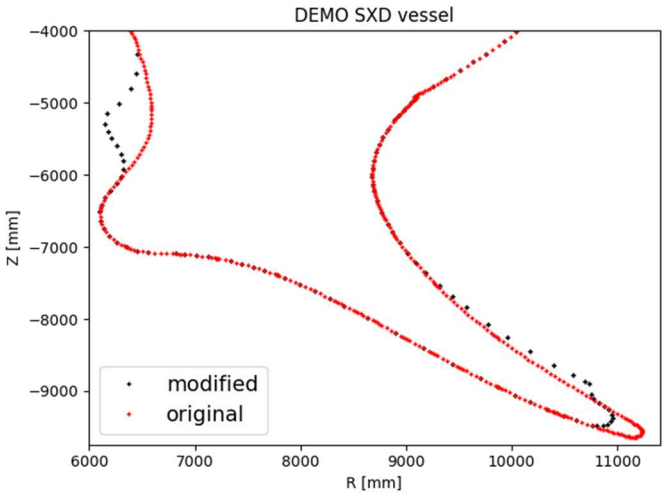

Figure 9: The adaptation of vacuum vessel structure to ensuring orthogonality of gridding (see Figure 10) near the target surface.

With this modification, a mesh of 120x36 for the SX configuration was generated successfully for use in the simulation, see Figure 10. The mesh satisfies the requirement that the power decay length at the low field side midplane of about 3 mm is resolved by 5-6 radial grid points. The radial width of the grid is 7 cm in the SOL and 10 cm in the core (at the outer midplane).

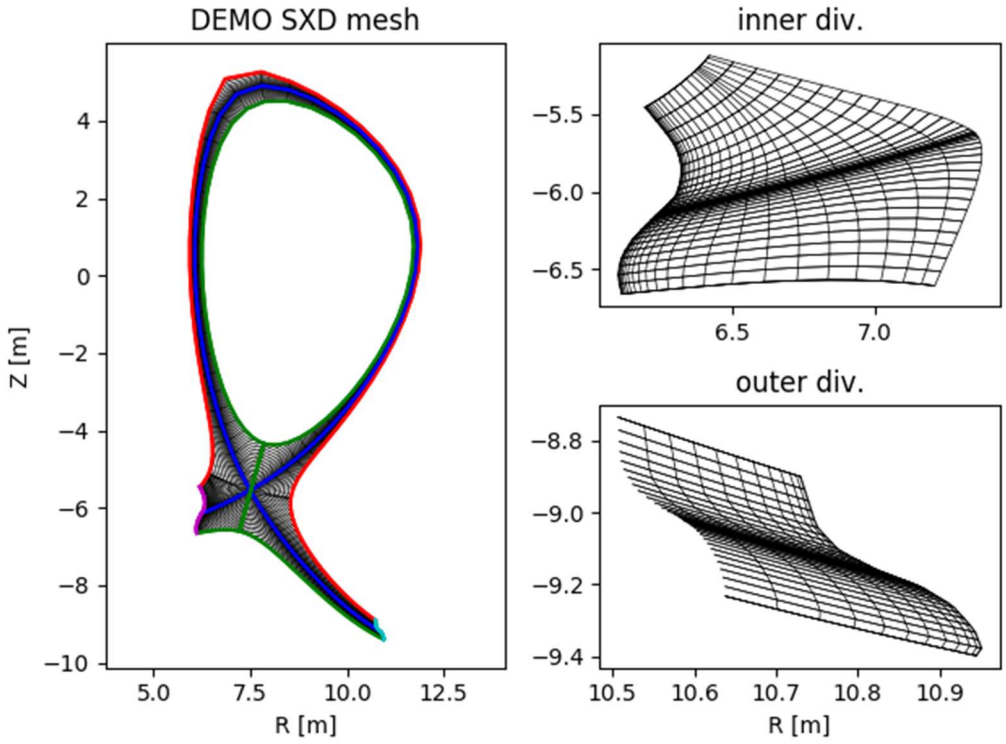

Figure 10: Computational mesh of DEMO SX configuration with modified vessel structure in physical space

The second issue was that with the insufficient specification of the density boundary condition at the core boundary, which resulted in oscillating plasma solution. This problem was fixed by setting the core boundary condition to BCCON=13, together with a feedback control strength parameter CONPAR=1e-2.

The third issue relates to the observations that the parallel current was not conserved flowing from one target to the other. This was due to the radial anomalous electric conductivity being too large by default (cfsig = 1e-3 in b2ah.dat). This was subsequently tuned to appropriate value (cfsig = 1e-5).

1.2.3.2 Runs and operational space

Fuelling and seeding scan was carried out, targeting at exploring numerically the operating space of DEMO in this configuration. The operating space is defined here by $T_{t,max}$ <= 5eV, n_{esep} <= $0.6n_{GW}$. Target peak heat load (required to be below 10 MW/m^2) turns out to be a looser constraint than $T_{t,max}$. From Figure 11 we observe that the operating space can be achieved either by increasing fuelling, hence increasing the main plasma density or by increasing argon seeding, i.e. increasing argon concentration. By increasing argon seeding rate in the scan, a maximum of 50% of P_{heat}=150 MW was radiated by argon, dominantly in the divertor region.

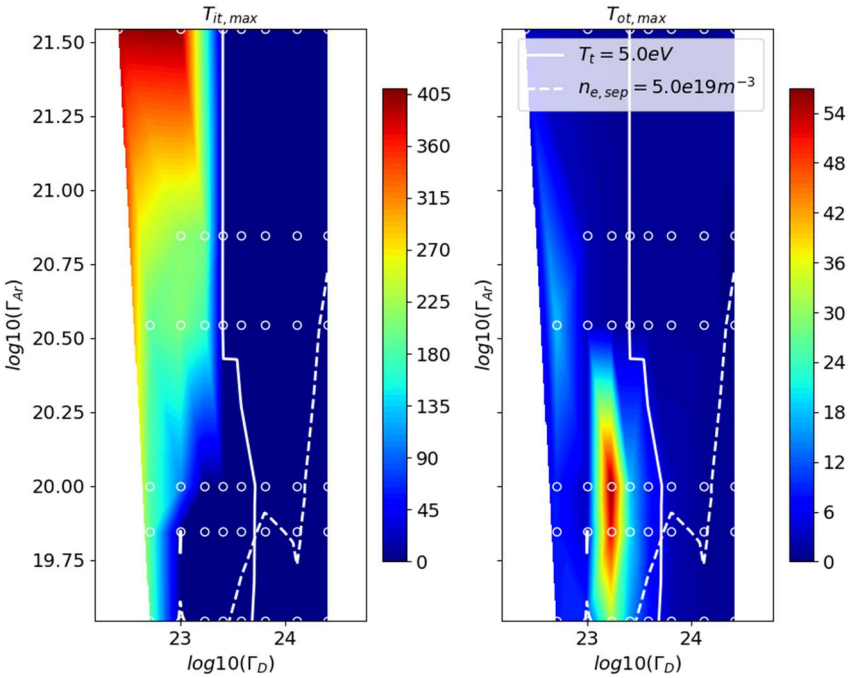

Figure 11: Peak T_e at inner and outer target of each 'matrix scan' point of fuelling and argon seeding scan. The area enclosed by the solid and dash line is the operating space defined by setting constraints of $T_{t,max}$ <= 5eV, n_{esep} <= $0.6n_{GW}$.

The physical parameter shown here is the peak T_e at the inner/outer target. The two targets were asymmetric especially outside the operating space, and in those conditions the asymmetry was found to cause and be enhanced by the thermoelectric current flowing between the two targets. This current transports heat from the cold end to the hot target. This current also affects the power distribution between inner and outer divertor. It is also seen in SX configuration that for the cases inside the operating space, this thermoelectric current flows predominantly from the outer target towards the inner, tilting the power distribution between outer/inner divertor above the ratio predicted by the 2-point model, as shown in Figure 12.

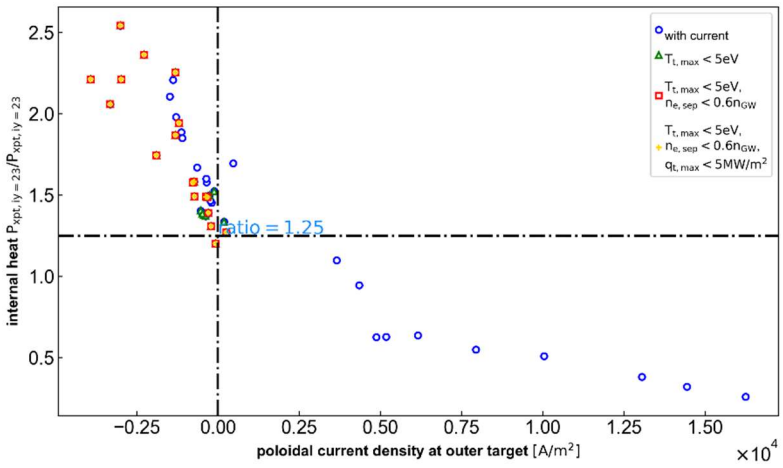

Figure 12: The ratio of the power distribution between the outer and inner divertor as function of the thermoelectric current. Positive current flows from the inner target to the outer, and negative current vice versa. The horizontal line is the ratio predicted by the 2-point model.

1.2.4 DN

1.2.4.1 Mesh and other configuration-specific settings

The mesh used in the SOLPS-ITER simulations for the DEMO DN is shown in Figure 13. The radial width of the mesh is 9 cm in the core and 7 cm in the SOL at the outer midplane. The figure shows modifications made to the wall geometry for the purpose of creating the computational mesh. In both divertors, the divertor throat opening was made larger compared to the engineering design, as otherwise orthogonality constraints prevented the grid creation. These changes were discussed with the engineering team. From the physics point of view, the changes may affect the divertor closure and this should be kept in mind for the analysis. Another configuration-specific problem was the creation of cells with a very narrow poloidal width in the core regions above and below the lower and upper X-points, respectively. These were associated with numerical problems in particular in simulations with significant Ar impurity concentrations. The solution was to increase the poloidal distance between the grid points along the separatrix near the X-points.

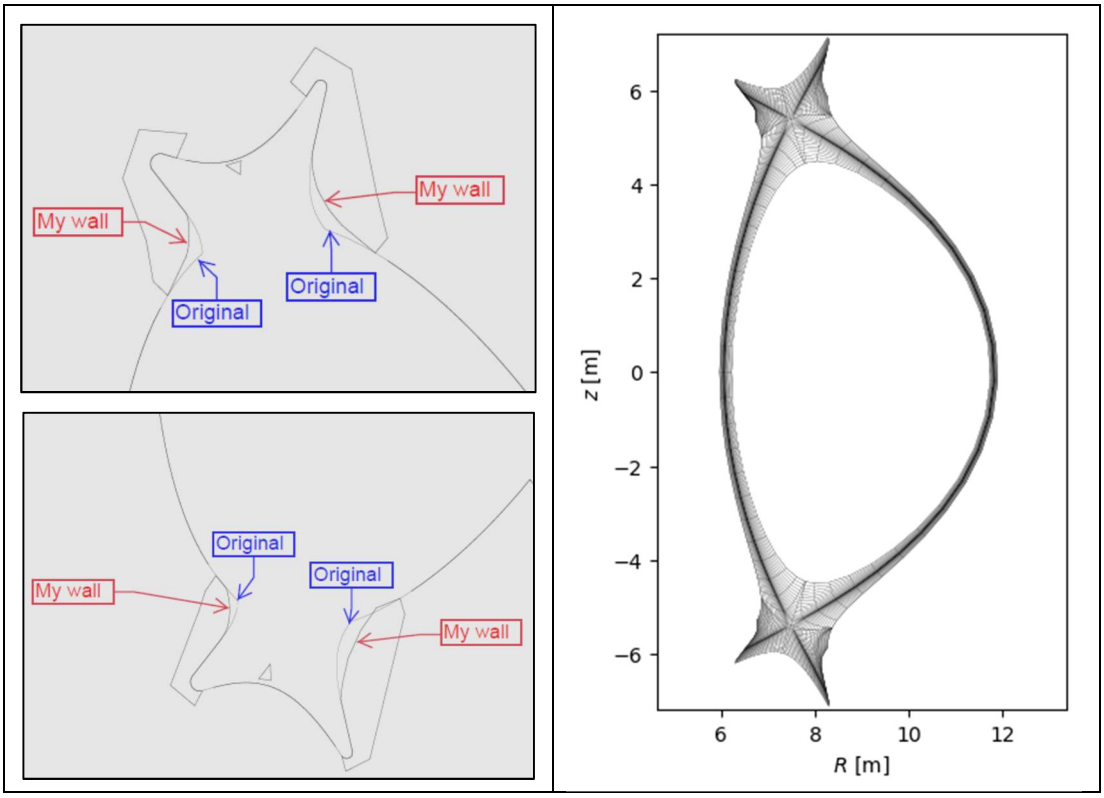

Figure 13: Computational mesh for the DEMO DN configuration (right). The two plots on the left indicate the differences between the original wall geometry obtained from the engineering activity ("Original") and the wall geometry used for the simulations ("My wall").

1.2.4.2 Runs and operational space

Figure 15 shows the maximum target temperatures obtained in the cases with significant Ar seeding simulated within the 2019 ADC activity. In these cases, the outer midplane D gas puff was operated with a feedback on the upstream separatrix density, as this was initially observed to yield faster converged solutions. In addition, a small, constant D gas puff (9.5E21 1/s) was placed on the inner midplane. The figures show an up-down asymmetry in the peak target temperatures, and the operational space is limited rather symmetrically (in-out) by the peak temperatures at the two lower targets. However, this does not give a full picture of the asymmetries in the DN configuration, as at low seeding rates the in-out asymmetries can be stronger than the up-down asymmetries, and also drifts can have a large influence on the asymmetries. The radiated power fraction varies within the operational space from 60% to 80%.

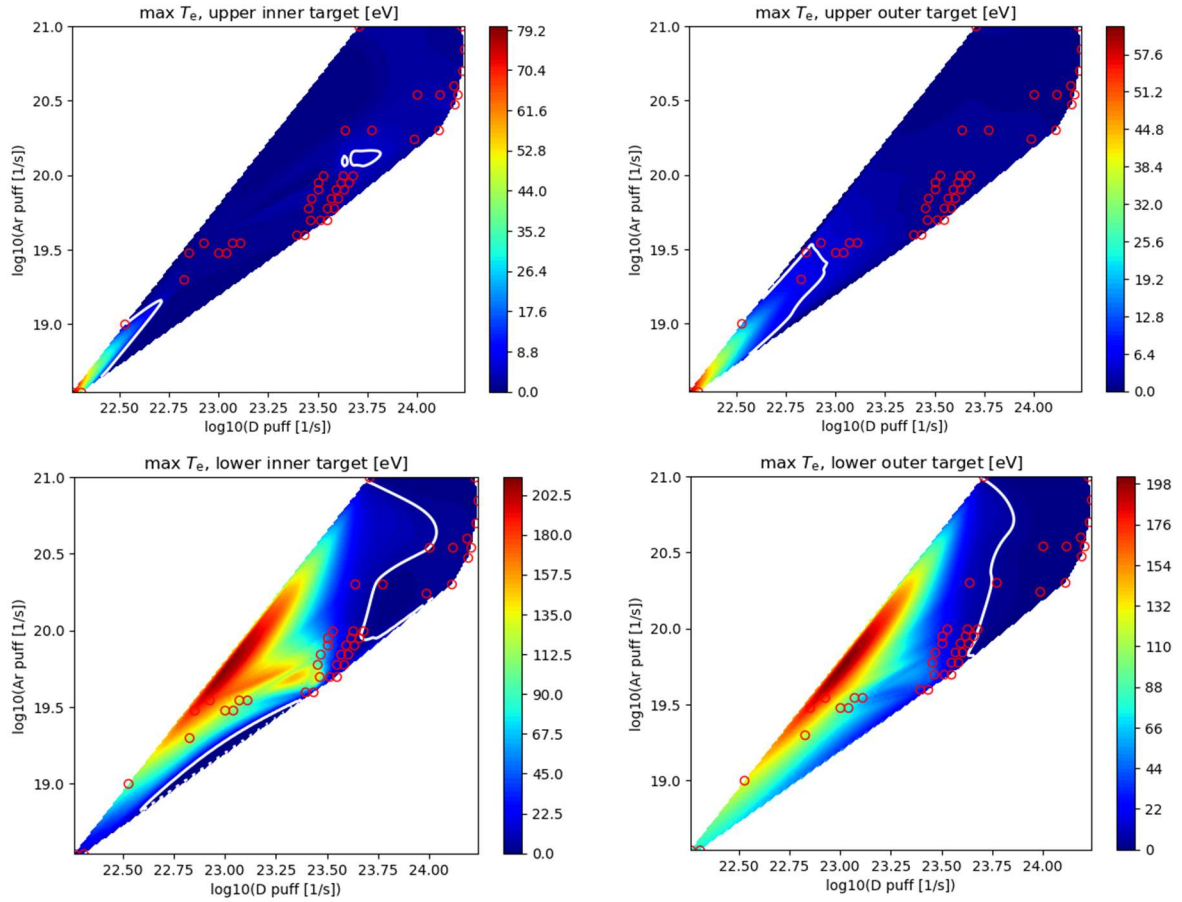

Figure 14: Maximum target temperatures (eV) in the DEMO DN configuration, for a range of D and Ar gas puff values. The red circles indicate simulated points and the white solid lines are the 5 eV contour lines for the target in consideration. All simulated cases have $n_{e,sep} < 0.6 n_{GW}$.

1.2.5 SF-

1.2.5.1 Mesh and other configuration-specific settings

The default SOLPS-ITER package does not provide tools to construct computational grids for snowflake configurations. The grid creation (219 poloidal x 29 radial cells) was instead performed using routines developed by Tilmann Lunt. First simulations using fluid neutrals, carried out by Mirko Wensing, showed poor numerical stability due to difficulties in approaching a physical plasma state. These problems were solved by first evolving the core plasma keeping the scrape-off layer frozen, followed by an evolution of the SOL keeping the core frozen. Once the plasma profiles approached a physically realistic state we activated the evolution of the different regions. Presently, the snowflake simulations show no particular geometry-related numerical instabilities.

1.2.5.2 Runs and operational space

To date, nine converged cases are obtained for the SF- configuration at low Ar seeding rates ($f_{rad} < 0.36$, average Ar concentration $< 0.5\%$) for which a possible operation point is not yet identified. While the heat exhaust conditions are met for three out of four targets, strike point 4 exceeds the material limits (see figure below). Increasing the distance between the two X-points would probably help to redistribute more power to SP2, but overall the mechanisms for power sharing between the four strike point regions are not yet fully understood and also drifts could play an important role. Present activities focus on extending the simulation database towards

cases with higher Ar-seeding to obtain a possible operation point and the setup of cases with kinetic neutrals. Furthermore, we presently assess the adaption of the X-point position and/or transport coefficients.

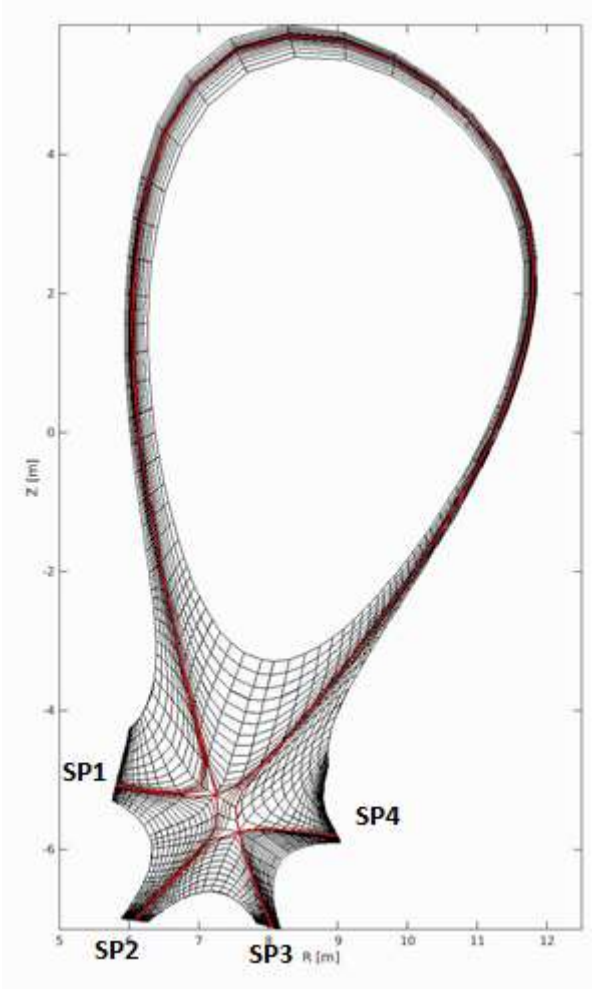

Figure 15: Computational mesh for the DEMO SF- configuration

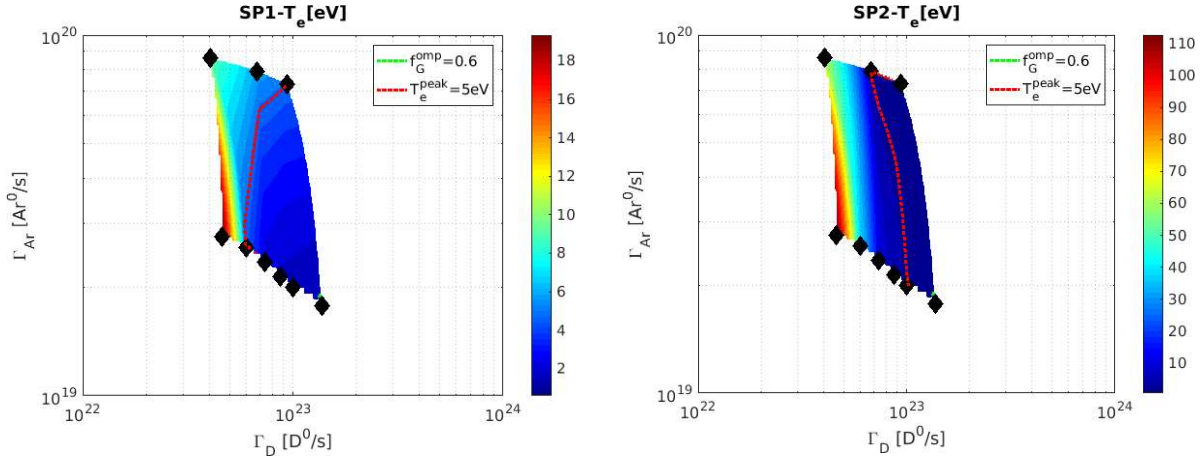

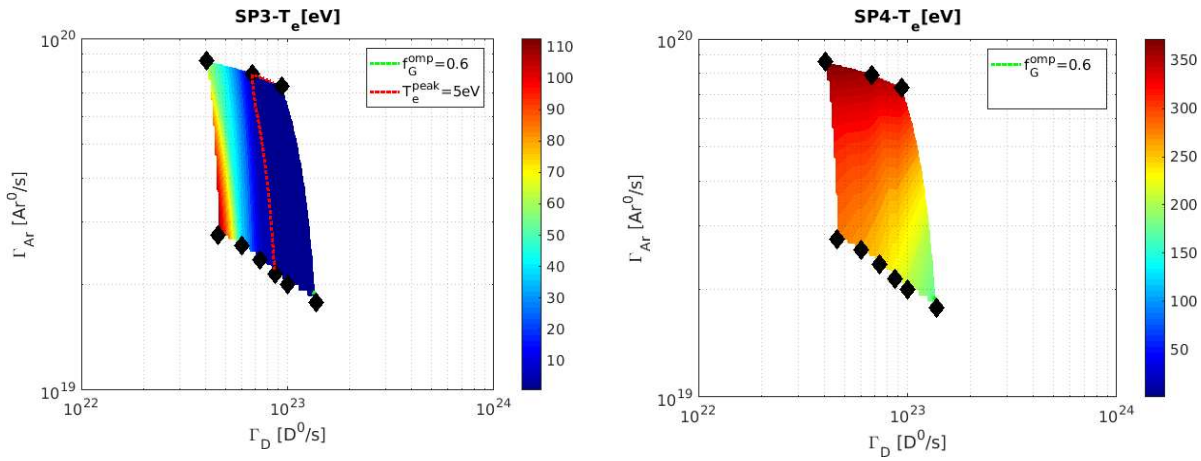

Figure 16: Maximum target temperatures (eV) in the DEMO SF- configuration, for a range of D and Ar gas puff values. The black diamonds indicate simulated points, the red dashed lines are the 5 eV contour lines for the target in consideration, and the green dashed lines indicate the $n_{e,sep} = 0.6n_{GW}$ boundary.

1.3 Conclusions and next steps

From the results shown in section 1.3 one can identify possible operational points satisfying the criteria $T_{e,target} < 5$ eV, $q_{target} < 10$ MW/m^2 and $n_{e,sep} < 0.6n_{GW}$ in all configurations apart from the SF-. The reason why there are no converged solutions for SF- in this regime is technical, as these simulations turned out to be challenging and not enough cases could be established with a high Ar seeding rate in 2019. Having a sufficiently high Ar seeding rate was observed to be crucial to obtain operational points in all of the other configurations, and no unseeded solutions were found within the operational spaces.

It is noteworthy that all of the configurations yield asymmetric target conditions, despite drifts being switched off. In the SN configuration, the outer target is significantly hotter than the inner target in most of the cases included in the parameter scan. The operational space is limited by the outer target temperature, whereas at the inner target the temperature is below 2 eV throughout the scan. In the XD configuration, the asymmetry is reversed, and the inner target becomes much hotter than the outer target in most of the simulations. The outer target temperature is below 2 eV throughout the scan, which implies a very efficient outer target temperature mitigation by the divertor geometry. In XD, the problem of heat exhaust in the outer divertor appears to be solved at the expense of the inner target.

In the SX configuration, the asymmetries evolve depending on the gas puff and Ar seeding level. It is also not as clear as in the previous two configurations which target is the critical one, as both targets can get temperatures above 5 eV at simulation points just outside the boundaries of the operational space. In the DN configuration, the operational space is limited rather symmetrically by the temperatures at the two lower targets, but there is a significant up-down asymmetry that should be verified and understood. In the SF- configuration, the highest temperatures are obtained at the outermost strike point.

In 2020, it is foreseen to extend the characterization and comparison of the operational spaces and analyse the causes of the asymmetries observed in all of the ADCs modelled in 2019. Future efforts should also consider the effects of kinetic neutrals and drifts on the asymmetries and for verification of the operational spaces.

2 Budget and roles

The table below shows the original ppy allocation and the main responsibilities of each association. All group members have participated in planning the work and analyzing the results together as a team.

Research Unit	roles	2019 ppy
CCFE	SX simulations (L. Xiang, D. Moulton)	0.45
ENEA	SN and XD simulations (F. Subba)	1.0
EPFL	SF- simulations (M. Wensing)	0.30
IPP	SOLPS support, activity management (D. Coster, T. Lunt, M. Wischmeier)	0.25
VTT	DN simulations, activity management (L. Aho-Mantila)	0.30